Applied Catalysis B: Environmental 311 (2022) 121351

Contents lists available at ScienceDirect

Applied Catalysis B: Environmental

journal homepage: www.elsevier.com/locate/apcatb

# Critical thinking on baseline corrections for electrochemical surface area (ECSA) determination of Pt/C through H-adsorption/H-desorption regions of a cyclic voltammogram

Raghunandan Sharma [a,*], Saso Gyergyek [b], Shuang Ma Andersen [a,*]

[a] Department of Green Technology, University of Southern Denmark, Odense M 5230, Denmark
[b] Department for Materials Synthesis, Jozef Stefan Institute, Ljubljana 1000, Slovenia

ARTICLE INFO

*Keywords:*
ECSA
Baseline correction
H adsorption/desorption
Carbon corrosion
AST

ABSTRACT

Determination of the electrochemical surface area (ECSA) of platinum supported on carbon (Pt/C) electrocatalysts through the hydrogen adsorption/desorption region has been revisited. Conventionally, ECSA is calculated by using the area of the H-adsorption ($H_{ad}$), H-desorption ($H_{de}$) or both of the regions to calculate the corresponding charge. Use of an appropriate baseline for the double-layer region is highly important for accurate determination of the associated charge. Unlike pure platinum, where a horizontal baseline for double-layer region is appropriate, the Pt/C catalysts have a skewed baseline for the double-layer region due to presence of surface functional groups from the support carbon. The skewness is not similar for the negative-going (cathodic) and the positive-going (anodic)scans, leading to significantly different $H_{ad}$ and $H_{de}$ charges. Again, the baselines from carbon may vary significantly during the catalyst durability study through an accelerated stress test (AST), due to oxidation of the support carbon. Present study investigates the effects of the baseline contribution on the ECSA calculations of Pt/C. It is observed that the baseline contribution for charge calculation (i) depends on the nature of the carbon support with significantly higher values (~10 fold) for $H_{de}$ as compared to that for $H_{ad}$ and (ii) increases for both the regions with the number of stress cycles during an AST. Hence, for Pt/C catalysts, while using a constant current baseline as a close approximation of the true baseline, charge associated to $H_{ad}$ should be used for calculation of ECSA to access the catalyst activity as well as the durability in terms of %ECSA loss during AST.

## 1. Introduction

Nanoparticulate Pt supported on carbon (Pt/C) is the *state-of-the-art* electrocatalyst for the polymer electrolyte membrane (PEM) fuel cells and the PEM electrolyzers [1–3]. Owing to their high electrocatalytic activity and high durability, the Pt or Pt-alloy supported on carbon or other materials remain interesting from both the scientific and technological points of view [4–6]. Studies aiming further development of such electrocatalysts frequently focus on high catalyst durability [7–10], low catalyst loading [11,12], recycling of critical materials from spent electrocatalysts [13–15], and optimization of electrode (ionomer/catalyst/support) interface structure [8,16,17]. Such studies on the Pt based electrocatalysts essentially include assessment of their initial electrochemical activity in terms of the electrochemical surface area (ECSA). Determination of the ECSA of such electrocatalysts is one of the important steps towards benchmarking their electrocatalytic performance [18].

Electrocatalytic activity of Pt/C is studied primarily through measurement of ECSA using reversible adsorption/desorption of certain species such as Cu, CO, H, etc. on the Pt surface during cyclic voltammetry in an electrolyte containing the desired species to be adsorbed/desorbed [19–22]. The charge associated with the adsorption or desorption region is used to calculate the specific ECSA [23–25]. However, among the reported species, use of hydrogen as the adsorption/-desorption species is advantageous for determination of ECSA of Pt/C. The H-adsorption ($H_{ad}$) and H-desorption ($H_{de}$) peaks can be observed without introduction of toxic gases (e.g. CO) or metal ions (e.g. $Cu^{2+}$) in the electrolytes. Further, apart from the fact that the access to CO is often limited due to safety reasons, use of such large species (compared to H) might underestimate the ECSA of Pt/C due to inaccessibility of the

* Corresponding authors.
*E-mail addresses:* rash@igt.sdu.dk (R. Sharma), mashu@igt.sdu.dk (S.M. Andersen).

https://doi.org/10.1016/j.apcatb.2022.121351
Received 9 November 2021; Received in revised form 21 March 2022; Accepted 24 March 2022
Available online 29 March 2022

Pt nanoparticles located inside the pores of the high surface area carbon support.

Ideally, for a monolayer deposition of hydrogen, both the $H_{ad}$ and $H_{de}$ peaks should have identical associated charges above the double-layer region as baseline, leading to identical values of ECSA. Studies have reported the ECSA values determined through either or both of the $H_{ad}$ and $H_{de}$ peaks [18,24–27] without a clear explanation for the choice. However, the assumption of a constant double-layer baseline holds good only for pure Pt showing no irreversible reactions in an impurity-free electrolyte [24,28]. Especially, while studying durability of supported Pt electrocatalysts (e.g. Pt/C) through potential cycling, ECSA values have often been used as a parameter to measure electrocatalytic activity. However, the double-layer baseline may not remain constant during accelerated stress test (AST) due to corrosion of the support carbon in the $H_{ad}$ and/or $H_{de}$regions [7,29–31]. The variation in the double-layer baseline may lead to incorrect assessment of the catalyst durability.

Effect of the baseline selection on the ECSA of Pt/C determined using the $H_{ad}$ and/or $H_{de}$regions has not been studied explicitly. This becomes highly important while studying the evolution of catalytic activity of Pt/C during an AST, where the carbon support degradation may affect the baseline significantly. Here, we attempt to quantify the baseline effects on the ECSA measurement on the Pt/C electrocatalysts. As it is known that the structure of carbon support may affect the Pt/C durability significantly [32], the present study includes several Pt/C catalysts supported on different types of carbon supports. Quantification of the contributions from baselines on the ECSA values determined using $H_{ad}$ and $H_{de}$regions is used further to suggest best protocol for routine and high throughput ECSA determination of Pt/C for various electrochemical studies. Effects of the baseline variations during an AST have also been investigated in detail.

## 2. Experimental methods

### 2.1. Materials

A total of three carbon supports and four Pt/C samples were used for the study. All the carbon supports, chosen from the commercially available carbons, namely Vulcan XC 72, Ketjenblack EC300J (KB300) and Ketjenblack EC600JD (KB600), were used as received. The two commercially available Pt/C samples, namely Pt/C-H9100 (~60 wt% Pt supported on high surface area carbon such as KB300 or equivalent; Johnson Matthey's HiSPEC™ 9100), Pt/C-BASF (~25 wt% Pt supported on Vulcan XC72 carbon; BASF) were also used as received. Pt/C-KB300 and Pt/C-KB600 were the home synthesized catalysts (synthesized using MW-assisted polyol route, as described in earlier reports from our group and others) [33–36] consisting of ~60 wt% Pt supported on KB300 and KB600, respectively. The Pt loading values (wt%) on support carbon were measured using thermogravimetric (TG) analysis. For comparison, Pt disc electrode (5 mm diameter) coated with Pt-black ($Pt_{Black}$; Johnson Matthey's HiSPEC™ 1000) was also studied. Table 1 summarizes the physicochemical and electrochemical properties of the studied catalysts. Electrolyte was prepared by diluting sulfuric acid (EMSURE® grade, assay > 95 – 97%, Merck, Germany) using ultrapure water (Milli-Q; resistivity ≥ 18.2 MΩ·cm at 25 °C). For catalyst ink preparation, isopropanol (HPLC grade) and 5 wt% Nafion® solution (Ion Power, Dupont D521) were used along with the ultrapure water.

### 2.2. Physical characterizations

Transmission electron microscope (TEM) imaging of the Pt/C samples was performed using a JEOL JEM-2010 F TEM. X-ray diffraction (XRD) patterns of the Pt/C samples were recorded using a Rigaku Miniflex 600 X-ray diffractometer equipped with a Cu K α ($\lambda = 1.5418$ Å) X-ray source. The average crystallite size ($L$) values, calculated using the Scherrer's formula ($L = 0.9\lambda/\beta Cos\theta$), with λ, θ and β respectively being the X-ray wavelength for Cu $K_\alpha$, the angle of diffraction and the FWHM (2Δθ) of the diffraction peak. The Pt(111) diffraction peak was used to determine the $L$ values, where the FWHM of the peak was estimated by fitting the peak using a Gaussian distribution. Specific surface area of the Pt/C and the carbon support samples were determined through nitrogen adsorption/desorption measurements using a Metromeritics® surface area and porosity analyzer (TriStar II PLUS). The BET surface area ($S_{BET}$) was calculated by using the adsorption isotherm (relative pressure values between 0.05 and 0.3). Finally, TG analysis of the Pt/C samples was performed using a NETZSCH STA449 F3 thermal analyzer. To avoid spontaneous combustion of the high Pt loading (~60 wt% Pt) Pt/C samples, a novel test protocol was developed. Instead of the frequently used procedure where the sample is heated from room temperature to a high temperature (800–1000 °C) in presence of oxygen (or a mixture of oxygen and nitrogen), the Pt/C sample (~6 mg) was first heated to 900 °C at a temperature scan rate of 10 °C/min in nitrogen atmosphere ($N_2$ flow rate: 20 mL/min). At 900 °C, the gas atmosphere was changed to a mixture of oxygen and nitrogen with their respective flow rates of 4 and 16 mL/min while cooling the furnace at a rate of 10 °C/min. This led to combustion of the Pt/C without a spontaneous/uncontrolled combustion. The residual weight at room temperature was used for determination of the Pt loading.

### 2.3. Electrochemical studies

Electrochemical measurements on the electrocatalysts (bulk Pt, Pt-black and Pt/C) were performed using a Zahner®IM6e electrochemical workstation. A standard three-electrode setup equipped with an $Hg/Hg_2SO_4$ (REF 601 Radiometer®) reference electrode (RE), a graphite rod (ϕ=5 mm) counter electrode and a working electrode (WE) prepared by modifying a glassy carbon (GC) rotating disc electrode (RDE; ϕ=5 mm; Pine instruments) by the catalyst. Before the catalyst loading, cleaning of the RDE was performed by polishing with the 0.5 μm alumina slurry followed by ethanol rinsing. For studies on pure Pt, a Pt-disc RDE (ϕ=5 mm; Pine instruments) coated with $Pt_{Black}$ catalyst was used as the WE. Typical catalyst inks were prepared by dispersing the catalyst powder in a stock solution consisting of ultrapure water, isopropanol and 5 wt% Nafion® solution (79.6, 20, 0.4 volumetric ratio), by ultrasonication (Hielscher UP200St ultrasonic homogenizer) for 60 s. The catalyst/stock solution ratios for the Pt/C and the Pt-black catalysts were kept as 2 mg/mL and 1.2 mg/mL, respectively. To study the variation of the carbon support baseline during AST, catalyst inks were also prepared for the corresponding support carbons. The carbon/solvent ratios for the carbons corresponding to the Pt/C catalysts with ~25 wt% Pt and ~60 wt% Pt were set to 1.6 and 0.8 mg/mL, respectively, to keep the concentration of carbon in the support ink identical to that for the corresponding catalyst ink. Working electrodes for the Pt/C or the support carbon inks were prepared by using GC RDE,

**Table 1**
Summary of the physical properties of the studied Pt/C catalysts and corresponding carbon supports.

| Sample | Carbon support | Pt wt% from TG | BET SA of carbon ($m^2/g$) | BET SA of Pt/C ($m^2/g$) | Crystallite size (nm) | ECSA ($m^2/g$) |
|---|---|---|---|---|---|---|
| Pt/C-BASF | Vulcan | 26.6 | 238 | 148 | 3.0 | 62.0 |
| Pt/C-H9100 | KB300 | 61.2 | 842 | 227 | 2.7 | 80.7 |
| Pt/C-KB300 | KB300 | 63.6 | 842 | 297 | 1.6 | 80.6 |
| Pt/C-KB600 | KB600 | 59.8 | 1408 | 527 | 1.8 | 102.5 |

while Pt-disc RDE was used for the Pt-black ink. For WE preparation, 10 μL of an ink was drop-casted on the electrode tip and dried at room temperature by continuous spinning at 700 rpm. The electrode preparation protocol for Pt/C electrocatalysts is well optimized, as reported elsewhere [18,37]. However, for carbon support, preparation of the inks and electrodes for AST have not been optimized. Here, we have used the procedure optimized for Pt/C. However, the prepared electrodes show reproducible cyclic voltammograms during AST, as demonstrated in Fig. S1.

The initial Pt loading on the GC RDE was measured by using a Thermo Scientific Niton XL3t GOLDD+ X-ray fluorescence (XRF) analyzer using an in-home calibration and method for the same (details can be found elsewhere [37]). The electrochemical measurements were performed in 1 M sulfuric acid (saturated with nitrogen), unless otherwise stated. The potentials measured w.r.t. the $Hg/Hg_2SO_4$ RE were converted to their corresponding values w.r.t. reversible hydrogen electrode (RHE) for reporting.

Linear sweep cyclic voltammetry was used for catalyst activation, ECSA measurement and durability study. Activation of the WE was performed by potential cycling for 20 cycles between 0.020 and 1.2 V at a scan rate of 100 mV/s. Effect of scan rate on the $H_{de}/H_{ad}$ area ratios was studied by recording cyclic voltammograms for 2 cycles between 0.02 and 1.2 V at different scan rates of 10, 50, 100, 200, 400 and 500 mV/s. Further, AST was performed by potential cycling between 0.4 and 1.6 V at a scan rate of 1 V/s, with the number of stress cycles ($N$) being 1600. Intermittent recording of cyclic voltammograms (2 cycles) between 0.02 and 1.2 V at a scan rate of 10 mV/s (observational cycles) after the $N$ values of 0, 20, 100, 200, 300, 400, 500, 600, 800, 1000, 1200, 1400 and 1600. The potential range for stress cycling was selected for accelerated degradations of both the Pt and the carbon support. The second cycle of the recorded observational cyclic voltammogram was used for ECSA calculation using the $H_{ad}$ and $H_{de}$ regions. The carbon support samples were also subjected to an electrochemical treatment identical to that for the Pt/C samples to study the baseline evolution during AST.

Evolutions of the $H_{ad}$ and $H_{de}$ areas for Pt/C and the corresponding carbon support baselines with the $N$ values were studied by measuring areas of different regions shown in Fig. 1. The regions ${H_{ad}}^{Pt/C}$and ${H_{ad}}^{C}$ correspond respectively to the apparent hydrogen adsorption on Pt and the reduction of functionalities on carbon surface. Similarly, the regions ${H_{de}}^{Pt/C}$and ${H_{de}}^{C}$ correspond respectively to the apparent hydrogen desorption from Pt and the reduction reactions on the carbon surface. Net areas corresponding to the hydrogen adsorption and desorption regions, i.e., ${H_{ad}}^{Net}$ and ${H_{de}}^{Net}$, were calculated using Eqs. (1 and 2), respectively. For the analysis, the potential window for all the regions was selected to be between 0.4 V (double-layer region) and 0.05 V. The lower limit of the potential window was such that it remains well above the hydrogen evolution region for all the voltammograms at different stress cycles, to avoid any contribution from hydrogen evolution or hydrogen oxidation reaction. In this study, it is assumed that the carbon support baseline remains unaffected by presence of the Pt nanoparticles. Finally, the anodic and cathodic peaks centered around ~0.6 V, labeled as $Q_{Ox}$ and $Q_{Red}$ in Fig. 1, are assigned respectively to hydroquinone oxidation and quinone reduction. The extent of carbon support corrosion during AST was monitored through measuring the area under the hydroquinone oxidation peak ($Q_{Ox}$) at ~0.65 V.

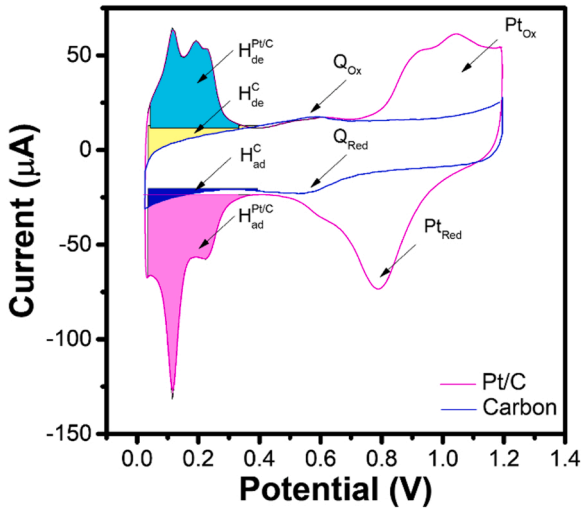


**Fig. 1.** Cyclic voltammograms of Pt/C (HiSPEC 9100; black solid line) and carbon (KB600, dotted red line) in $N_2$-saturated 1 M sulfuric acid at a can rate of 10 mV/s. The areas of interest for the ECSA analysis have been shown as shaded regions.

$$H_{ad}^{Net} = H_{ad}^{Pt/C} - H_{ad}^{C} \quad (1)$$

$$H_{de}^{Net} = H_{de}^{Pt/C} + H_{de}^{C} \quad (2)$$

For comparison, ECSA of typical Pt/C sample was also determined by Cu underpotential deposition (Cu-upd). For Cu-upd, Pt/C modified GC RDE, activated in 1 M sulfuric acid as described above, was subjected to potential cycling in an electrolyte consisting of 1 M sulfuric acid and 2 mM CuSO4. Cyclic voltammograms were recorded at a scan rate of 10 mV/s between 0.02 and 1.2 V. As holding at lower potential (0.02 V) led to bulk deposition of Cu, a continuous scan for 2 cycles was performed and the Cu stripping peak of the second cycle was used to determine the ECSA. The surface charge densities of 210 and 407 μC/cm$^2$ were used for H adsorption and Cu-upd on polycrystalline Pt, respectively [25]. Carbon monoxide (CO) stripping, another typical method to estimate the ECSA of Pt [21,25], could not be explored because of accessibility limits arising from safety reasons.

## 3. Results and discussion

### 3.1. Physical characteristics of the materials

Support carbons and Pt/C samples covering broad range of physicochemical properties, as summarized in Table 1, have been explored. TEM images and XRD patterns of the three carbon support samples, i.e. Vulcan XC72, KB300 and KB600, have been shown in Fig. 2. The carbon samples consist of spherical grains measuring in between 10 and 30 nm in diameter. Observation of grains at higher magnification shows that the grains of Vulcan XC72 carbon are smooth and compact while, those of KB300 and KB600 appear hollow, wrinkled and some of them broken (indicating them being increasingly porous, respectively). This is also reflected from their BET surface area (Table 1), with KB600 showing the highest value. Again, the XRD patterns of the carbon samples exhibit their amorphous nature [38] with no significant crystallinity difference among the studied carbon samples. The broad diffraction peaks correspond to diffractions from different graphitic planes as indicated in Fig. 2d [39]. The studied support carbons consist of different oxygen functional groups such as HO-C═O, C-O-C/C═O/C-OH, as observed using X-ray photoelectron spectroscopy on Vulcan carbon in our earlier study [40]. These functional groups may act as active sites for Pt nanoparticle nucleation during synthesis as well as for the electrochemical redox reactions involving adsorption/desorption of different species.

All the studied Pt/C catalysts (commercial and homemade) show electrocatalytic activities (in terms of ECSA) comparable to state-of-the-art electrocatalysts for PEMFC cathodes. As revealed from the TEM images shown in Fig. 3, the Pt/C electrocatalysts consist of Pt nanoparticles (~2 nm) supported on their corresponding carbon supports. All the Pt/C catalysts show uniform distribution of the Pt nanoparticles. The particle size and their distribution on carbon for Pt/C-KB300 and Pt/C-

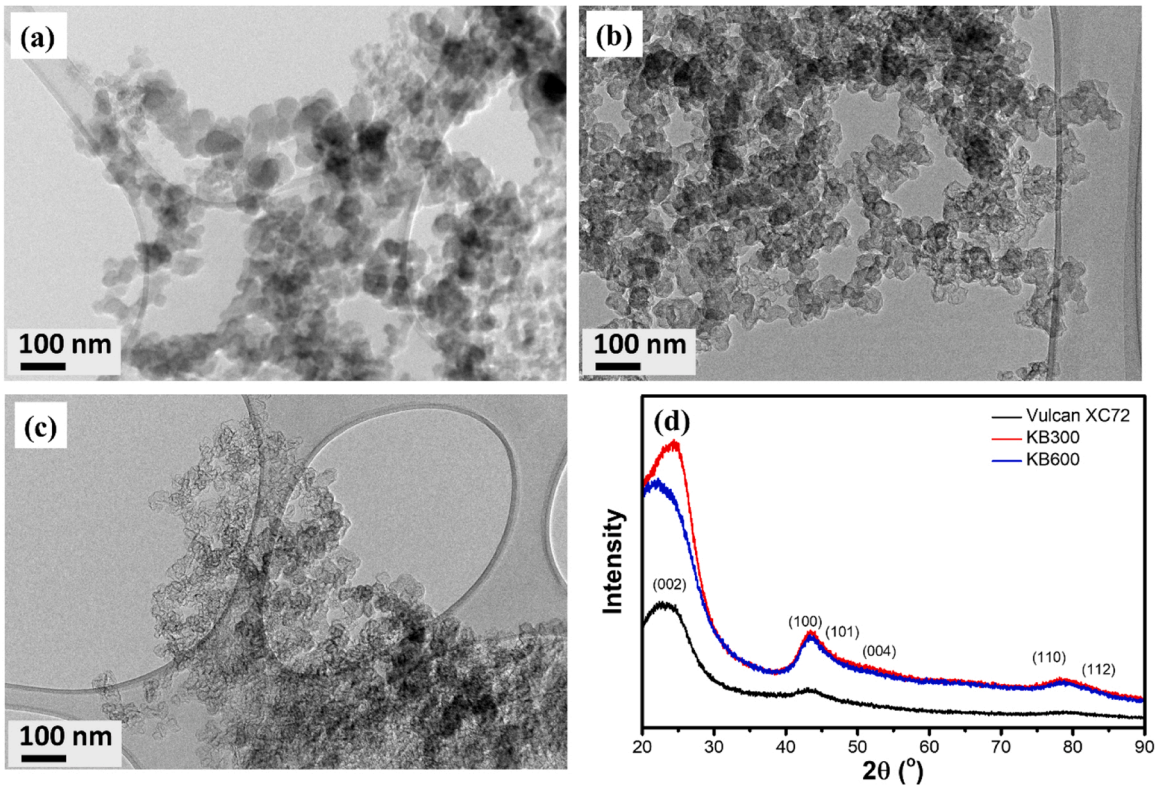


**Fig. 2.** TEM images of (a) Vulcan XC72, (b) KB300 and (c) KB600. (d) shows the XRD patterns of the three carbon samples.

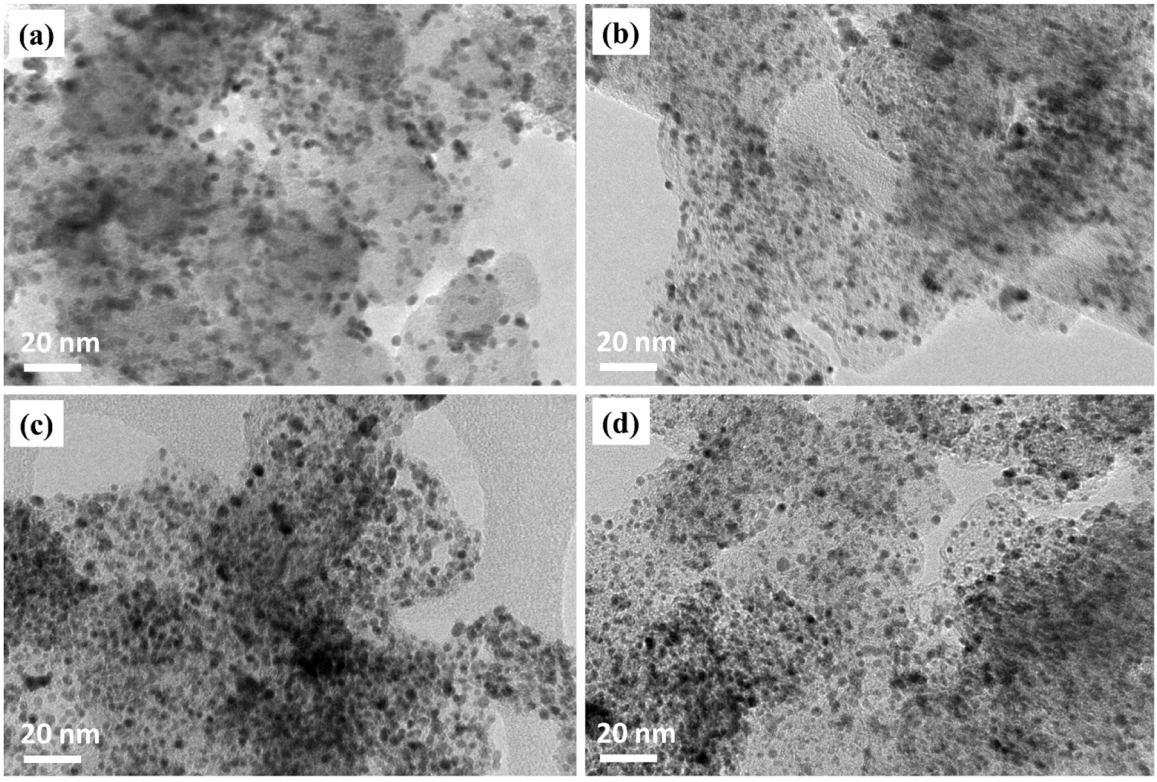


**Fig. 3.** TEM images of (a) Pt/C-BASF (b) Pt/C-H9100, (c) Pt/C-KB300 and (d) Pt/C-KB600 showing homogeneous dispersion of Pt nanoparticles (dark contrast) on the corresponding support carbons.

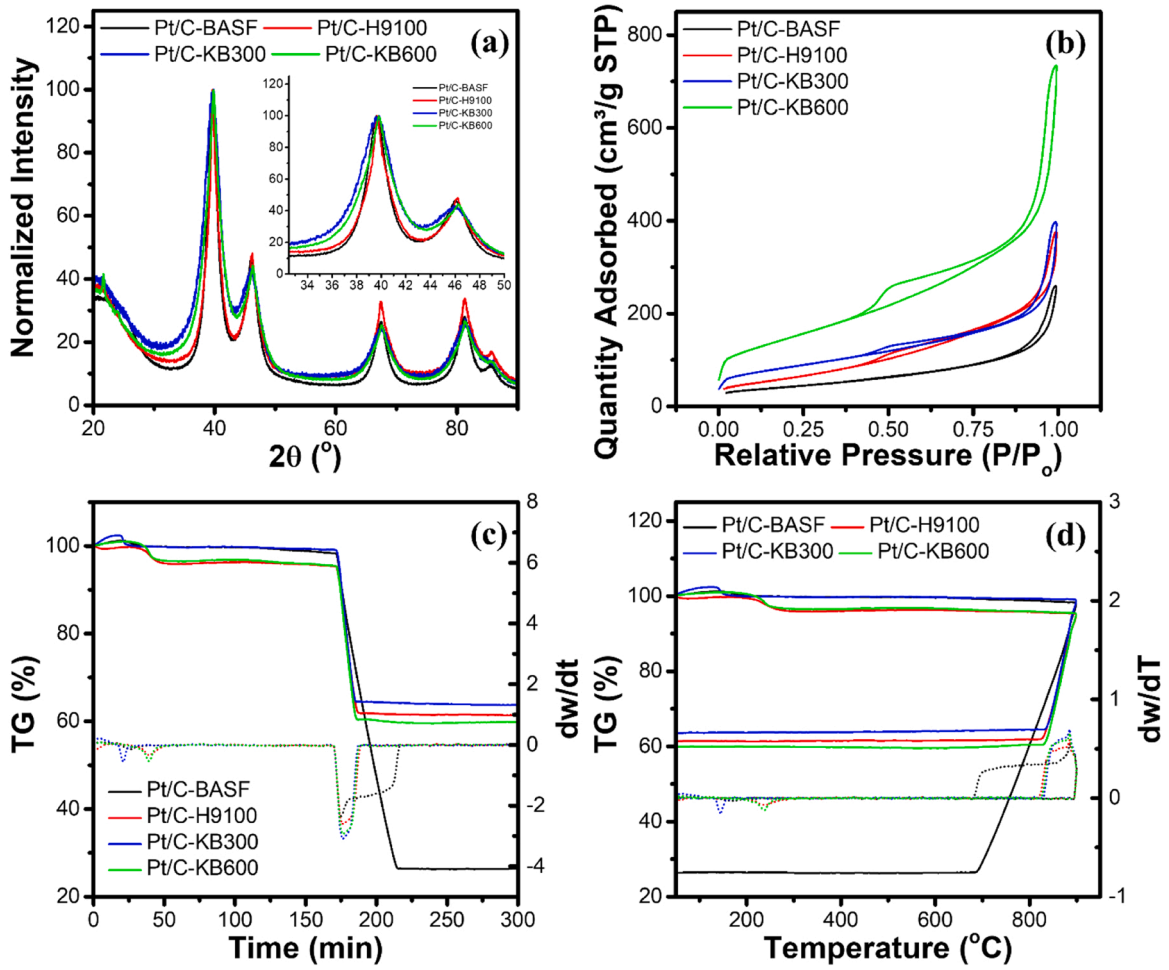


**Fig. 4.** (a) XRD patterns, (b) nitrogen adsorption-desorption isotherms, (c) TG (%weight vs time) and differential TG (dw/dt; first derivative of the TG plot) and (d) TG (%weight vs temperature) and differential TG (dw/dT; first derivative of the TG plot) for the studied Pt/C samples. of the studied Pt/C samples. Inset of (a) shows magnified view of the XRD patterns exhibiting Pt(111) and Pt(200) diffraction peaks.

KB600 are comparable to those for their commercial counterpart (Pt/C-H9100), except to the slightly high areal density of Pt nanoparticles for Pt/C-KB300.

Further, XRD patterns of the Pt/C samples shown in Fig. 4a exhibit the characteristic diffraction peaks for nanoparticulate Pt. Diffraction peak at 2θ values ~39.7°, 46.4°, 67.7°, 81.3° and 85.7° correspond respectively to the (111), (200), (220), (311) and (222) planes from Pt, while the broad peak ~20° is attributed to the amorphous support carbon. The average crystallite size (*L*) values, calculated using the Scherrer's formula have been shown in Table 1. The highest value of *L* for Pt/C-BASF also corresponds well with its lowest initial ECSA value. Further, nitrogen adsorption-desorption isotherms of the Pt/C catalysts have been shown in Fig. 4b. The isotherms resemble to the type-IV category, characteristic to mesoporous materials [41]. The corresponding BET surface area values for the Pt/C catalysts and the corresponding support carbons have been listed in Table 1, where Pt/C-KB600 and KB600 show the highest values for the catalysts and the carbon supports, respectively. TG analysis of the Pt/C samples (Fig. 4c-d) confirms the Pt loading values of the Pt/C catalysts to be close to 60 wt% for Pt/C-H9100, Pt/C-KB300 and Pt/C-KB600, while ~27 wt % for Pt/C-BASF (Table 1).

### 3.2. Carbon corrosion during AST

Corrosion of carbon is well-known during the fuel cell operation and the electrochemical studies exploring the catalyst performance and durability [7,29,42–45]. Carbon corrosion during the AST in liquid electrolytes leads to build-up of the quinone-hydroquinone redox peaks in the double-layer region of the cyclic voltammogram (~0.5 to ~0.8 V) [29–31,46]. Typical linear sweep voltammograms for support carbon (Vulcan XC72) and Pt/C electrocatalyst (Pt/C-BASF) throughout the AST shown in Fig. 5a exhibit the evolution of the hydroquinone oxidation peak at ~0.65 V. It is clear that the peak intensity increases with increasing the value of *N*, which can be attributed to the increasing concentration of quinone/hydroquinone due to carbon corrosion. Variation of the area under the quinone peak shown in Fig. 5b suggests higher carbon corrosion in case of Pt/C, as compared to that of bare carbon support. The peak area and hence the quinone/hydroquinone concentration gets saturated with increasing *N*.

The varying intensity of the quinone-hydroquinone redox peak makes the double-layer region baseline correction for ECSA determination inaccurate due to variable contribution of the redox peak in the plateau double-layer region. Also, the contributions from carbon support in the $H_{ad}$ and $H_{de}$ regions vary dramatically during AST, leading to inaccurate determination of ECSA when double-layer region baseline correction is used. Hence, it is worthy to quantify the effect of carbon support baseline correction of the variation of ECSA values obtained using the $H_{ad}$ and $H_{de}$ regions.

### 3.3. Effect of baseline correction on ECSA and durability assessments

Evolution of cyclic voltammograms of the commercial and synthe-

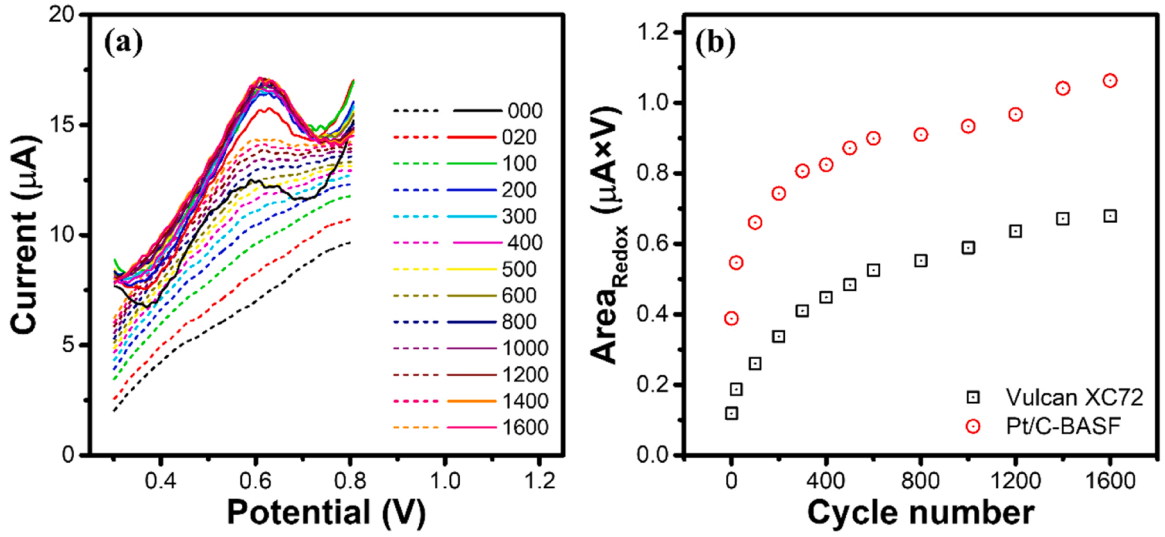


**Fig. 5.** (a) Linear sweep voltammograms (scan rate: 10 mV/s, electrolyte: 1 M sulfuric acid) showing evolution of hydroquinone oxidation peak for Pt/C-BASF (solid lines) and Vulcan-XC72, the corresponding carbon support (dashed lines) during AST. (b) Evolution of the area under the hydroquinone oxidation peak for Pt/C-BASF and Vulcan-XC72 during AST.

sized Pt/C catalysts and their equivalent catalyst supports (carbon) during AST are shown in Fig. 6 and Fig. S2 (supporting information). Cyclic voltammograms for all the studied Pt/C samples evolve significantly during AST (Fig. S3, supporting information). The $H_{ad}$ and $H_{de}$ regions respectively for the cathodic and anodic scans below ~0.4 V diminish with the $N$ value. Similar evolutions can be observed for the Pt-oxide formation peak above 1.0 V during anodic scan and the peak ~0.8 V during the cathodic scan corresponding to reduction of Pt-oxides. On the other hand, the peaks corresponding to reduction and oxidation of surface functionalities on carbon that are observed respectively during the cathodic and anodic scans for carbon support below ~0.4 V, become prominent with increasing number of stress cycles, especially with a significant increase with increasing the number of stress cycles from 0 to 100. Interestingly, the double-layer currents, especially cathodic current for carbon support remain significantly lower compared to corresponding values for the concerned Pt/C. Both the cathodic and anodic scans show small peaks corresponding to the quinone/hydroquinone redox reaction [30] at ~0.6 V that increase with increasing number of stress cycles for both the carbon supports and the Pt/C catalysts, as discussed previously (Fig. 5). Although the intensities of the hydroquinone redox peaks are generally higher for Pt/C electrocatalysts as compared to those for the corresponding carbon support, the support carbon contributions in the $H_{ad}$ and $H_{de}$ regions may be considered unaffected by the presence/absence of Pt. Under this approximation, the voltammograms for carbon support may be used for baseline corrections in the in the $H_{ad}$ and $H_{de}$ regions.

Fig. 7a - d show variations of the areas of the $H_{ad}$ and the $H_{de}$ regions with the number of stress cycles ($N$) for all the four catalyst / support pairs studied. It is clear that for all of the studied Pt/C catalysts, the $H_{de}$ peak area values above the double-layer region baseline remain significantly lower compared to the corresponding $H_{ad}$ peak area below the double-layer region baseline, throughout the stress cycling. Hance, ECSA values calculated using the $H_{de}$ peak areas are underestimated significantly throughout the stress cycling and the rate of activity loss is observed to be faster, leading to apparently lower durability as compared to the corresponding values when $H_{ad}$ peak areas are used.

Interestingly, for the synthesized Pt/C samples, the support carbon baseline corrected area values for the two regions, i.e., $H_{ad}^{Net}$ and $H_{de}^{Net}$, correspond each other well for the entire range of $N$ values. This is unlike the corresponding values for the commercial Pt/C samples, where $H_{de}^{Net}$ values show smaller degradation with $N$ as compared to the corresponding $H_{ad}^{Net}$ values. The difference may be due to the fact that for the synthesized Pt/C samples, baseline corrections have been made using identical carbon samples, while for the commercial samples, the carbon support used in the catalyst may be slightly different (possibly different production batch, processing history, aging, etc.) than that used for the baseline correction. Moreover, in all cases, $H_{ad}^{Pt/C}$ is closer to or almost overlaps with $H_{ad}^{Net}$ comparing to $H_{de}^{Pt/C}$.

The ratios of the desorption and adsorption peak area values for the carbon support baseline ($H_{de}^{C}/H_{ad}^{C}$) and for the Pt/C catalysts using either horizontal double-layer region baseline ($H_{de}^{Pt/C}/H_{ad}^{Pt/C}$) or carbon support baseline ($H_{de}^{Net}/H_{ad}^{Net}$) provide information on the extent of the influence from carbon support baseline. Evolutions of the baseline corrections for support carbon, i.e., $H_{ad}^{C}/\ H_{ad}^{Pt/C}$ for $H_{ad}$ region and $H_{de}^{C}/\ H_{de}^{Pt/C}$ for $H_{de}$ region, with $N$ have been shown in Fig. 8a and b, respectively. Although both the $H_{ad}^{C}/\ H_{ad}^{Pt/C}$ and $H_{de}^{C}/\ H_{de}^{Pt/C}$ ratios increase with $N$, the latter shows an order of magnitude higher values, suggesting large impact of the carbon support baseline on the ECSA calculations and hence suggesting advantage of using the $H_{ad}$ region over the $H_{de}$ region. This is further observed from the variations of the $H_{de}^{C}/\ H_{ad}^{C}$ ratios during AST, which, as shown in Fig. 8c, varies between 2 and 5 for different carbon supports. Finally, variations of the $H_{de}/H_{ad}$ (double-layer region baseline) and $H_{de}^{Net}/H_{ad}^{Net}$ (carbon support baseline) ratios for different Pt/C catalysts with the $N$ values have been shown in Fig. 8d, along with the corresponding variation for the double-layer region baseline corrected $H_{de}/H_{ad}$ ratio for $Pt_{Black}$. It is clear that for all the Pt/C samples studied, the double-layer region baseline corrected values ($H_{de}/H_{ad}$) show larger variations with $N$, compared to the corresponding variations for those corrected with carbon support baseline ($H_{de}^{Net}/H_{ad}^{Net}$). For $Pt_{Black}$, the $H_{de}/H_{ad}$) remains ~1 ($H_{de} = H_{ad}$), while for the Pt/C samples, the $H_{de}^{Net}/H_{ad}^{Net}$ ratio varies between 0.95 and 1.1 with $N$. The variation of the $H_{de}^{Net}/H_{ad}^{Net}$ ratio with $N$ may be attributed to the fact that the carbon support baseline determined using the carbon support modified WE may not represent the real baseline of the catalyst nanoparticle supported carbon. In addition, it may not represent factors such as redox reactions involving trace impurities from electrolyte.

The baseline corrections have shown significant dependence on the type of carbon support. For example, Vulcan carbon (support for Pt/C-BASF) shows smallest value of $H_{de}^{C}/H_{ad}^{C}$, while it is observed to be the largest for KB600. Similarly, the ratio $H_{de}^{Pt/C}/H_{ad}^{Pt/C}$, which corre-

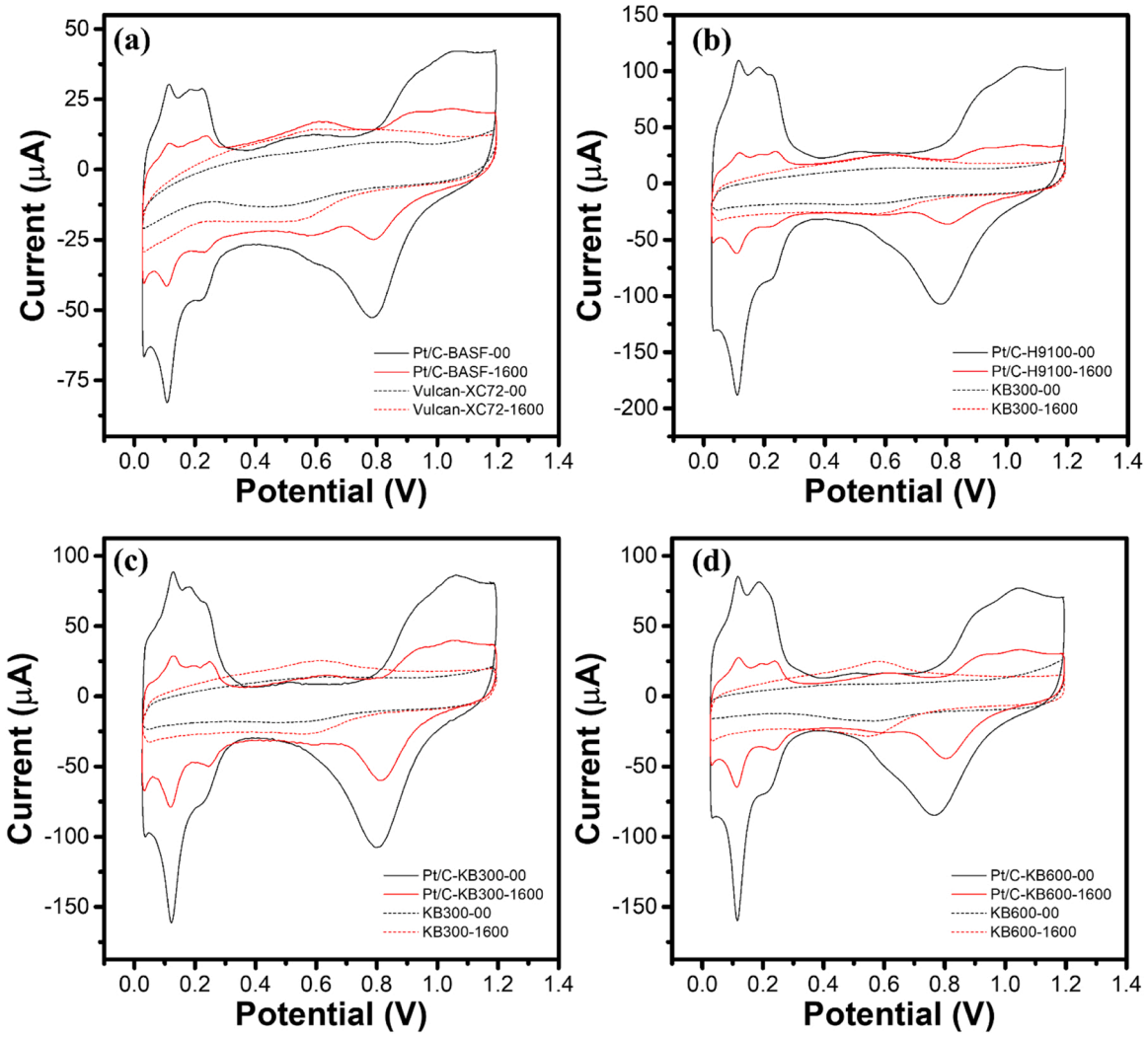


**Fig. 6.** Initial and final cyclic voltammograms of Pt/C catalysts and their corresponding support carbons, i.e., (a) Pt/C-BASF / Vulcan XC 72, (b) Pt/C-H9100 / KB300, (c) Pt/C-KB300 / KB300 and (d) Pt/C-KB600 / KB600, recorded during AST in $N_2$ asturated 1 M sulfuric acid. Cyclic voltammograms have been recorded at a scan rate of 10 mv/s. For the commercial Pt/C samples, i.e., Pt/C-BASF and Pt/C-H9100, Vulcan XC 72 and KB300 carbons have been assumed as the corresponding support carbons.

sponds to the ratio of the ECSA value calculated using the double-layer region baseline corrected area of the $H_{de}$ region to that using corresponding area of the $H_{ad}$ region, also varies between ~0.59 and ~0.88, depending on the type of carbon support. This may be correlated with the BET surface area values of the carbon supports as well as the catalysts (Table 1). The ${H_{de}}^{C}/{H_{ad}}^{C}$ and ${H_{de}}^{Pt/C}/{H_{ad}}^{Pt/C}$ ratios exhibit smaller values for the support carbons (or catalysts) having smaller BET surface area. On the other hand, the ratio ${H_{de}}^{Net}/{H_{ad}}^{Net}$, which corresponds to the ratio between the ECSA values calculated using the carbon support baseline corrected $H_{de}$ and $H_{ad}$ regions, has been found to vary between ~0.84 and 0.98. Hence, the ECSA values obtained from the $H_{de}$ and $H_{ad}$ regions correspond better to each other when the carbon support baselines are used to calculate the peak areas.

As the difference between areas under $H_{de}$ and $H_{ad}$ regions become insignificant when the support carbon baseline is used, one would expect an ideal situation with the said areas being equal ($H_{de} = H_{ad}$) if no carbon is used (e.g., $Pt_{Black}$ catalyst). The areas under $H_{de}$ and $H_{ad}$ regions (between 0.4 and 0.05 V) for the Pt-disc modified with $Pt_{Black}$ have been calculated using the observational cyclic voltammograms recorded during AST in 1 M sulfuric acid (Fig. S4, supporting information). For $Pt_{Black}$, the area under $H_{de}$ region remains marginally lower than that under the $H_{ad}$ region, leading to a $H_{de}/H_{ad}$ ratio of 0.99. This higher area for $H_{ad}$ region may be attributed to various side reactions involving reduction of impurities, evolution of hydrogen (in proximity of 0 V), etc. Although the additional current in $H_{ad}$ region remains nearly unaffected by the scan rate, hence leading to the $H_{de}/H_{ad}$ ratio ~1. Hence, selecting a double-layer region baseline leads to inaccurate determination of ECSA even if no catalyst support is involved. Apparently, use of the carbon support baseline nearly compensates the additional currents and leads to the $H_{de}/H_{ad}$ ratio ~1, providing more accurate determination of ECSA.

Further, the area corresponding to ${H_{ad}}^{Pt/C}$is less deviated from the carbon baseline corrected values (${H_{ad}}^{Net}$), as compared to the deviation of the ${H_{de}}^{Pt/C}$ values from ${H_{de}}^{Net}$. Quantitatively, the correction factors for the support carbon baseline, defined as the ratios between the corresponding areas for carbon support and Pt/C catalyst, i.e., ${H_{ad}}^{C}/{H_{ad}}^{Pt/C}$ for $H_{ad}$ region and ${H_{de}}^{C}/\ {H_{de}}^{Pt/C}$ for $H_{de}$ region, are observed to be dependent significantly on the support carbon type. The influence of correction from support carbon baseline remains 3–5 times higher for the $H_{de}$ region as compared to that for the $H_{ad}$ region. Hence, if a double-layer region baseline is applied for the ECSA calculations, the $H_{ad}$ region should be used over the $H_{de}$ region.

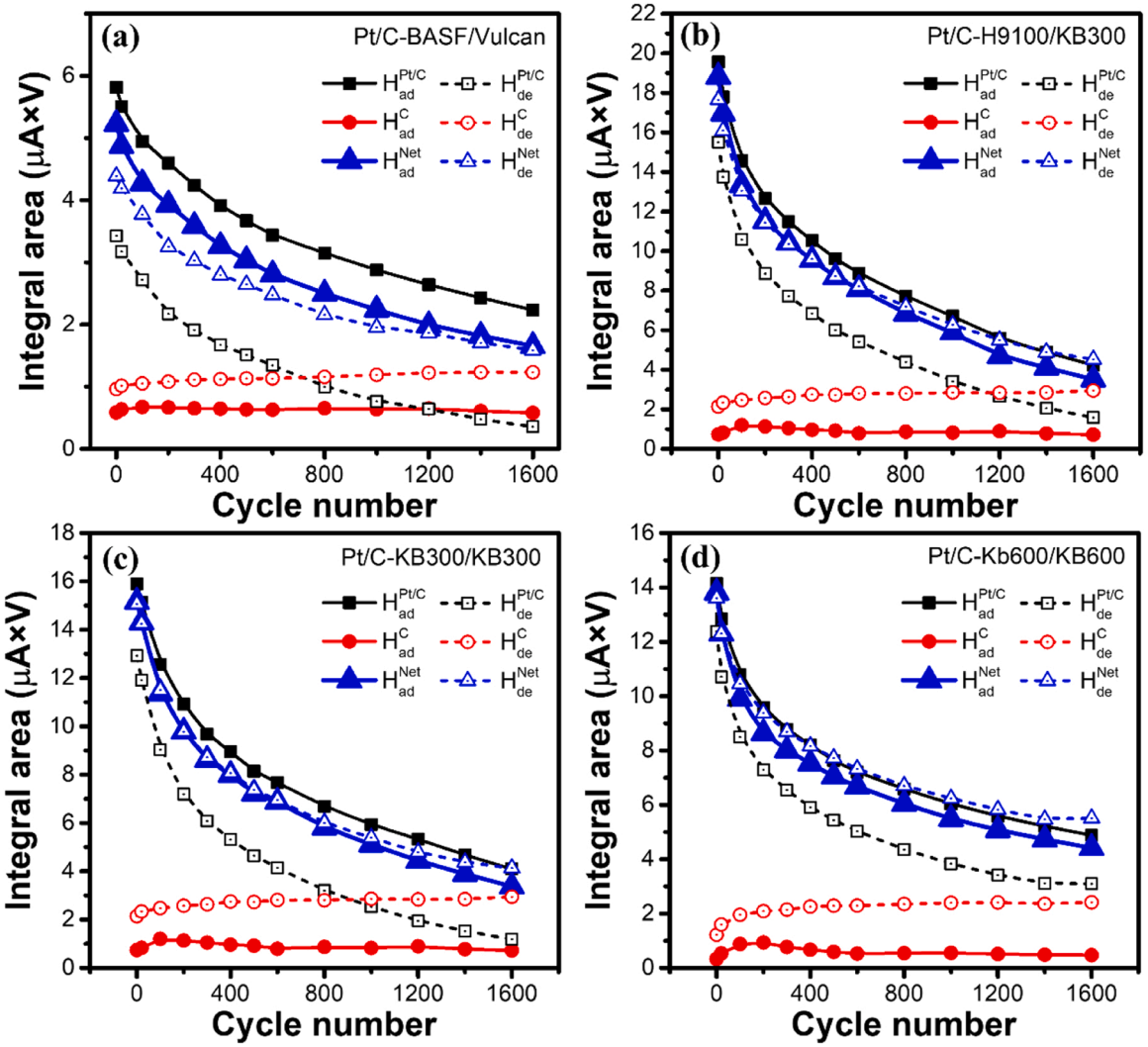


**Fig. 7.** Variations of the Pt/C catalyst and carbon support areas corresponding to $H_{ad}$ and $H_{de}$ regions with the cycle number ($N$) for (a) Pt/C-BASF and Vulcan XC 72, (b) Pt/C-H9100 and KB600, (c) Pt/C-KB300 and KB300 and (d) Pt/C-KB600 and KB600 catalyst and support systems. The net areas (carbon support baseline corrected) corresponding to $H_{ad}$ and $H_{de}$ regions are also shown.

### *3.4. Effect of scan rate on the areas of $H_{ad}$ and $H_{de}$ regions*

Cyclic voltammograms recorded at various scan rates can be used for ECSA calculations [21,47–50]. To study the effect of the scan rate on the areas of $H_{ad}$ and $H_{de}$ regions, cyclic voltammograms have been recorded at different scan rates ranging between 10 mV/s and 500 mV/s. The study has been carried out for both the pure (unsupported) Pt and Pt/C electrodes. For pure Pt, Pt-disc RDEs (φ = 5 mm) modified with Pt-black (HiSPEC 1000) has been used. Again, for Pt/C sample, GC RDE modified with the Pt/C-KB300 has been used, while the corresponding carbon support baselines have been recorded using a GC RDE modified with KB300. The cyclic voltammograms for Pt/C show characteristics similar to those for the pure Pt electrode, apart from the presence of the broad peaks corresponding to the quinone/hydroquinone redox reaction at ~0.6 V, as shown in Fig. 9a–b. The peak areas of the $H_{ad}$ and $H_{de}$ regions of the cyclic voltammograms corresponding to the pure Pt and the Pt/C electrodes, calculated using a double-layer region baseline, show linear variation with the scan rate (Fig. S5, supporting information). Also, the $H_{ad}$ and $H_{de}$ peak areas show small difference for the pure Pt electrode, as can be seen from the nearly overlapping plots. On the other hand, for Pt/C, the $H_{ad}$ and $H_{de}$ peak areas calculated using horizontal double-layer region baseline show significant difference with the $H_{de}$ peak area values being lower than their corresponding values for the $H_{ad}$ peak. However, the areas corrected using the carbon support baseline show nearly identical values, highlighting the advantage of choosing a more suitable baseline.

This is further elaborated in Fig. 9c, exhibiting the difference between the areas corresponding to $H_{ad}$ and $H_{de}$, i.e., $H_{ad} - H_{de}$, which remains approximately constant and small with the scan rate for the pure Pt electrode, while varies linearly for the GC RDE modified with Pt/C-KB300. Further, the variations of the $H_{de}/H_{ad}$ area ratios for different electrodes with the scan rate have been shown in Fig. 9d. When using the double-layer region baseline, the $H_{de}/H_{ad}$ area ratios for Pt/C show low values (<1) for slower scan rates and increase with the scan rate, reaching to the ideal situation, where $H_{de}/H_{ad} = 1$. For example, at a scan rate of 10 mV/s, the Pt/C electrodes show the area ratio of ~0.8.$Pt_{Black}$$H_{de}/H_{ad}$. The difference between $H_{ad}$ and $H_{de}$, even for pure Pt electrode, arises possibly due to additional currents from (i) reduction of trace amounts of the impurities adsorbed on electrode surface, (ii) evolution of hydrogen on pure Pt near a potential close to the standard redox potential for hydrogen evolution, etc. For example, the area difference $H_{ad} - H_{de}$ (0.22 μA×V) for blank GC RDE of geometrical area identical to that of the Pt disc electrode has been observed to be similar to that for the pure Pt electrode (0.28 μA×V). Cyclic voltammogram of the blank GC RDE showing the $H_{ad}$ and $H_{de}$ regions has been shown in Fig. S6 (supporting information). The small difference between the two

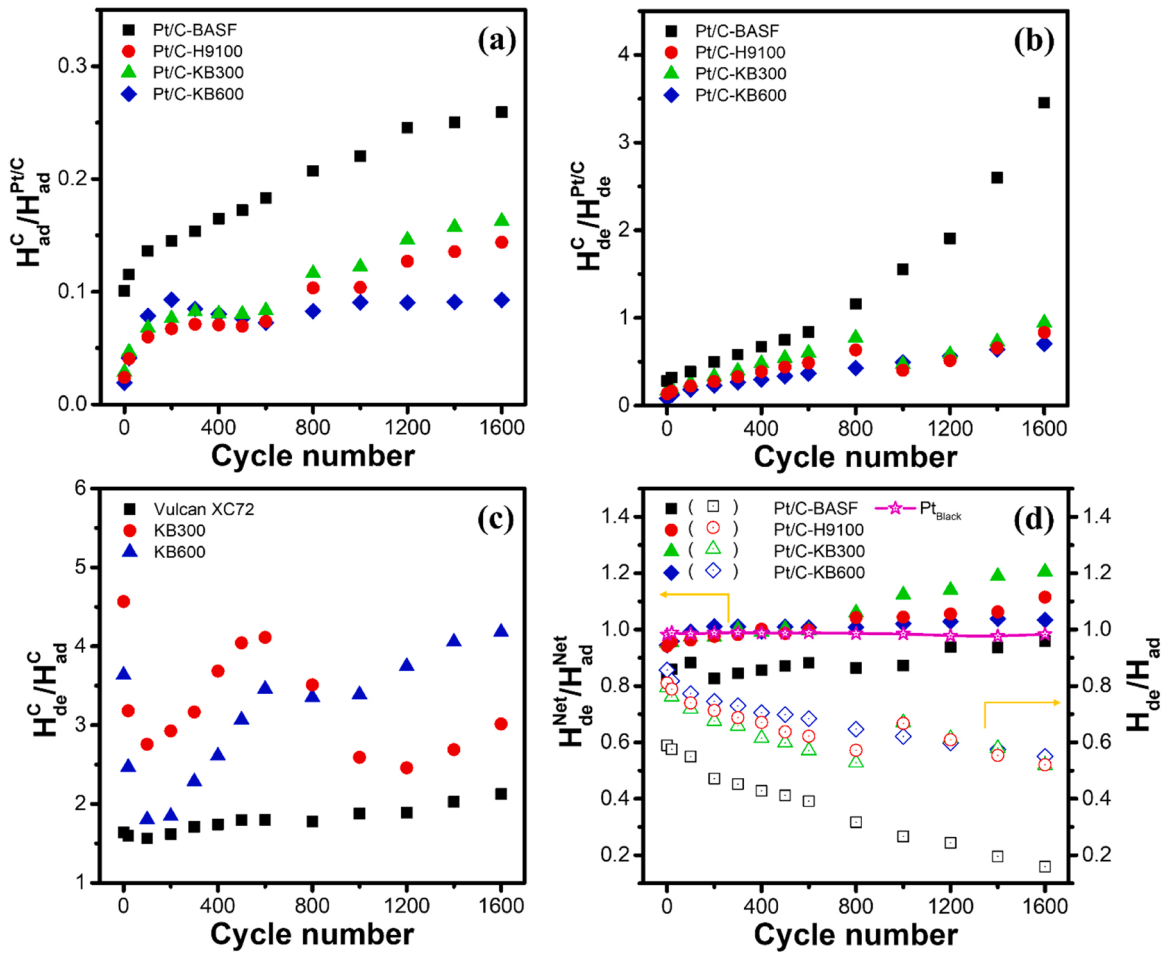


**Fig. 8.** Variations of the (a) $H_{ad}{}^{C}/\ H_{ad}{}^{Pt/C}$ (b) $H_{de}{}^{C}/\ H_{de}{}^{Pt/C}$ (c) $H_{de}{}^{C}/\ H_{ad}{}^{C}$ and (d) $H_{de}/H_{ad}$ (hollow symbols; double-layer region baseline) and $H_{de}{}^{Net}/H_{ad}{}^{Net}$ (solid symbols; carbon support baseline) ratios for different Pt/C catalysts and corresponding carbon supports with N values during AST. Variation of the double-layer region baseline corrected $H_{de}/H_{ad}$ ratio for $Pt_{Black}$ with the N values has also been shown in (d).

values for GC and pure Pt may be attributed to the fact that while for GC, the area difference ($H_{ad} - H_{de}$) arises merely due to monolayer adsorption of certain species on the GC surface, for pure Pt, catalytic reactions, i.e., hydrogen evolution in the $H_{ad}$ region also may contribute. However, use of $H_{ad}$ region is recommended for the ECSA calculations as the contribution from hydrogen evolution in $H_{ad}$ region appears much smaller compared to that from the carbon support baselines of the $H_{ad}$ and $H_{de}$ regions.

### 3.5. Comparison between ECSA values from to $H_{ad}$, $H_{de}$ and Cu-upd

Although we did not have an opportunity to compare our results with the CO stripping method, the fact that the ECSA estimation from $H_{de}$ region is underestimated despite selecting the slanted baseline, it is evident that selection of the carbon support baseline would improve the ECSA estimation. For a comparison with other methods of the ECSA determination, we have determined the ECSA of Pt/C by using the stripping of underpotentially deposited Cu ($Cu - upd$). Fig. 10 shows a comparison between these different methods. Cyclic voltammograms recorded in 1 M sulfuric acid without Cu (00 mM Cu) and with 2 mM $CuSO_4$ are shown in Fig. 10a. The two voltammograms have been recorded at a scan rate of 10 mV/s on same electrode (Pt/C-H9100 modified GC RDE; activated for 20 cycles in 1 M sulfuric acid). Different regions corresponding to $H_{ad}$, $H_{de}$ and $Cu-upd$ are marked. The ECSA values calculated using different integration regions have been shown in Fig. 10b. It is clear that the ECSA values calculated using the $H_{ad}$ and $H_{de}$ regions are much higher than that using the $Cu-upd$ region. This could be attributed to factors such as larger size of Cu leading to lower accessibility of the Pt surface in the porous carbon support for Cu as compared to that for $H^{+}$. Again, use of CO or Cu for intermittent determination of ECSA during AST of Pt/C may not be preferred as it would disturb the test. Moreover, the values from different methods may not be directly comparable due to porous structure of electrodes. Further, evolution of the carbon support baseline during AST affects the CO-stripping region as well, through evolution of the hydroquinone oxidation peak due to carbon corrosion.

Rigorous assessment of ECSA of nanoparticulate electrocatalysts has been debated frequently [51–53]. Moniri et al. have recently noted use of slanted baseline to be more appropriate over the horizontal baseline for determination of ECSA from $H_{de}$ region [52]. Furthermore, authors have compared the $H_{de}$ method with the CO-stripping, another frequently reported method for the ECSA determination of nanoparticulate electrocatalysts. Authors have noted that the ECSA is underestimated despite using the slanted baseline. Rudi et al. have noted similar results, suggesting underestimation of ECSA from $H_{de}$ area as compared to that from CO-stripping area [53]. Moreover, the baseline for CO stripping is also potential dependent and must be corrected for the same. Here, we suggest that instead of using a slanted baseline, use of a carbon support baseline (for both of the $H_{ad}$ and $H_{de}$ regions) may provide ECSA values for Pt/C electrocatalysts comparable to CO-stripping. It should be noted that use of the carbon support baseline provides similar ECSA values for both the $H_{ad}$ and $H_{de}$ regions and hence there is no preference between these two regions. However, the effect of carbon baseline correction is more for the $H_{de}$ region and

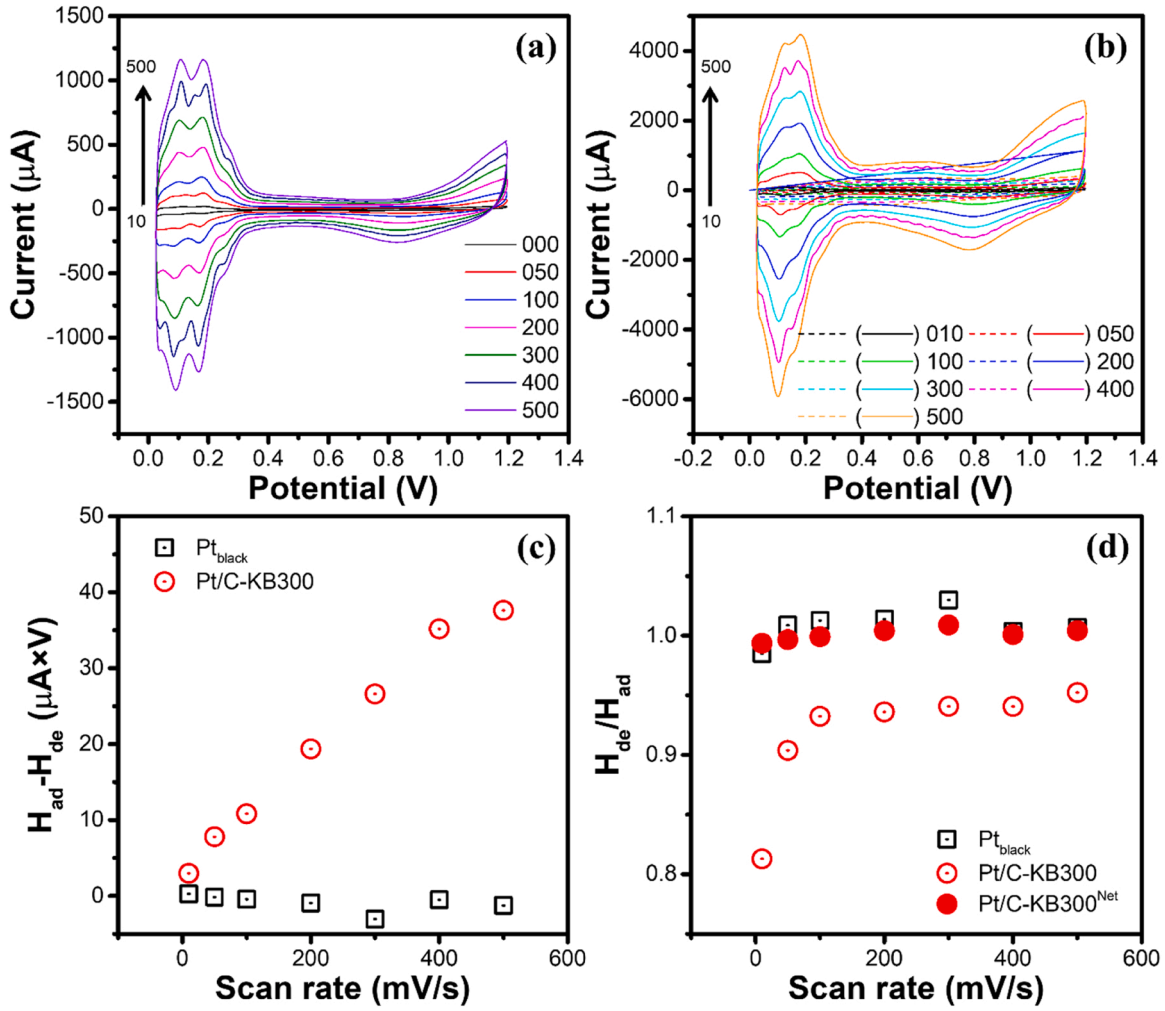


**Fig. 9.** Cyclic voltammograms of (a) platinized Pt-disc ($Pt_{Black}$) and (b) GC RDE modified with Pt/C-KB300 or KB300, recorded at varying scan rates between 10 mV/s and 500 min $N_2$ saturated 1 M sulfuric acid. (c) Scan rate vs. the difference between the areas corresponding to $H_{ad}$ and $H_{de}$, i.e., $H_{ad} - H_{de}$, for the $Pt_{Black}$ (square) and the GC RDE modified with Pt/C-KB300 (hollow circle). Double-layer region baselines have been used for both the electrodes. (d) Variations of the $H_{de}/H_{ad}$ area ratios with the scan rate for the $Pt_{Black}$ and the GC RDE modified with Pt/C-KB300 (hollow circle: using double-layer region baseline; solid circle: using carbon support (KB300) baseline).

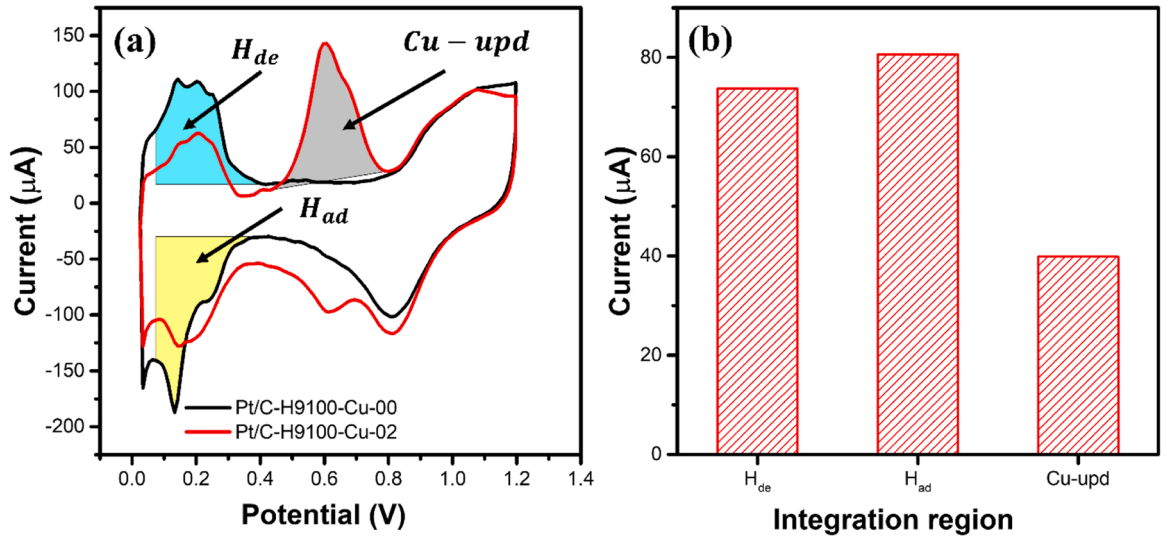


**Fig. 10.** a) Cyclic voltammograms recorded in 1 M sulfuric acid at 10 mV/s without Cu (00 mM Cu) and with 2 mM $CuSO_4$ (02 mM). The integration areas are shown shaded. (b) ECSA values calculated using different integration regions shown in (a).

hence, when horizontal baselines used, $H_{ad}$ region should be preferred.

### 3.6. Outlook

Present study assumes that the evolutions of support carbon contributions in the $H_{ad}$ and $H_{de}$ regions during AST may be considered unaffected by the presence/absence of Pt. Evolution of the hydroquinone oxidation peaks for during AST suggest higher oxidation of the carbon support in presence of Pt. This might indicate the carbon support baseline in presence of Pt being different than that of carbon support, which could be explored further to obtain more accurate baseline.

## 4. Conclusions

In conclusion, effect of baseline on determination of the ECSA of Pt/C through $H_{ad}$ and $H_{de}$ regions has been investigated. Conventional ECSA calculation using the horizontal double-layer region baseline overestimates the ECSA for $H_{ad}$ region while the ECSA for $H_{de}$ region is underestimated due to deviation of the carbon support baseline from the double-layer region. Moreover, the deviation between the two categories of the ECSA values increases with number of potential cycles during an AST, leading to apparently different degradation patterns. Here, we demonstrate that use of the carbon support baseline leads to similar degradation patterns and similar initial ECSA values for both the $H_{ad}$-based and the $H_{de}$-based ECSA calculations. The support carbon baseline correction factors for $H_{de}$-based ECSA calculations have been observed to be an order of magnitude higher than those for $H_{ad}$-based ones. Hence, in case of the ECSA calculation of Pt/C using a double-layer region baseline, the area of $H_{ad}$ region should rather be used as an appropriate approximation.

## CRediT authorship contribution statement

**Raghunandan Sharma**: Conceptualization, Methodology, Software, Validation, Formal analysis, Investigation, Data curation, Writing – original draft, Writing – review & editing; Visualization. **Saso Gyergyek**; Methodology, Investigation, Writing – review & editing. **Shuang Ma Andersen**: Conceptualization, Methodology, Writing – review & editing, Supervision, Resources, Project administration, Funding acquisition.

## Declaration of Competing Interest

The authors declare that they have no known competing financial interests or personal relationships that could have appeared to influence the work reported in this paper.

## Acknowledgments

The authors acknowledge Rikke Klindt Muller, IGT SDU for performing the surface area and thermogravimetry measurements. The authors also acknowledge the financial support from Innovation Fund Denmark, InnoExplorer Program, Nr. 9122-00112; Danish ESS Lighthouse on hard materials in 3D, SOLID, Grant number 8144-00002B; EnergiFyn udviklingsfond and Slovenian Research Agency (research core funding Nos. P2-0089).

## Appendix A. Supporting information

Supplementary data associated with this article can be found in the online version at doi:10.1016/j.apcatb.2022.121351.

## References

[1] M. Carmo, D.L. Fritz, J. Mergel, D. Stolten, A comprehensive review on PEM water electrolysis, Int. J. Hydrog. Energy 38 (2013) 4901–4934, https://doi.org/10.1016/j.ijhydene.2013.01.151.
[2] S. Sui, X. Wang, X. Zhou, Y. Su, S. Riffat, C.-j Liu, A comprehensive review of Pt electrocatalysts for the oxygen reduction reaction: nanostructure, activity, mechanism and carbon support in PEM fuel cells, J. Mater. Chem. A 5 (2017) 1808–1825, https://doi.org/10.1039/C6TA08580F.
[3] C. Zhang, X. Shen, Y. Pan, Z. Peng, A review of Pt-based electrocatalysts for oxygen reduction reaction, Front. Energy 11 (2017) 268–285, https://doi.org/10.1007/s11708-017-0466-6.
[4] M. Chourashiya, S. Gyergyek, S.M. Andersen, Solution combustion synthesized ceria or alumina supported Pt as cathode electrocatalyst for PEM fuel cells, Mater. Chem. Phys. 242 (2020), 122444, https://doi.org/10.1016/j.matchemphys.2019.122444.
[5] G. Cognard, G. Ozouf, C. Beauger, G. Berthomé, D. Riassetto, L. Dubau, R. Chattot, M. Chatenet, F. Maillard, Benefits and limitations of Pt nanoparticles supported on highly porous antimony-doped tin dioxide aerogel as alternative cathode material for proton-exchange membrane fuel cells, Appl. Catal. B Environ. 201 (2017) 381–390, https://doi.org/10.1016/j.apcatb.2016.08.010.
[6] C. Park, E. Lee, G. Lee, Y. Tak, Superior durability and stability of Pt electrocatalyst on N-doped graphene-TiO2 hybrid material for oxygen reduction reaction and polymer electrolyte membrane fuel cells, Appl. Catal. B Environ. 268 (2020), 118414, https://doi.org/10.1016/j.apcatb.2019.118414.
[7] Y. Zhang, S. Chen, Y. Wang, W. Ding, R. Wu, L. Li, X. Qi, Z. Wei, Study of the degradation mechanisms of carbon-supported platinum fuel cells catalyst via different accelerated stress test, J. Power Sources 273 (2015) 62–69, https://doi.org/10.1016/j.jpowsour.2014.09.012.
[8] S.M. Andersen, L. Grahl-Madsen, Interface contribution to the electrode performance of proton exchange membrane fuel cells – impact of the ionomer, Int. J. Hydrog. Energy 41 (2016) 1892–1901, https://doi.org/10.1016/j.ijhydene.2015.11.101.
[9] L. Dubau, L. Castanheira, F. Maillard, M. Chatenet, O. Lottin, G. Maranzana, J. Dillet, A. Lamibrac, J.C. Perrin, E. Moukheiber, A. ElKaddouri, G.D. Moor, C. Bas, L. Flandin, N. Caqué, A review of PEM fuel cell durability: materials degradation, local heterogeneities of aging and possible mitigation strategies, WIREs Energy Environ. 3 (2014) 540–560, https://doi.org/10.1002/wene.113.
[10] B. Li, D.C. Higgins, Q. Xiao, D. Yang, C. Zhng, M. Cai, Z. Chen, J. Ma, The durability of carbon supported Pt nanowire as novel cathode catalyst for a 1.5kW PEMFC stack, Appl. Catal. B Environ. 162 (2015) 133–140, https://doi.org/10.1016/j.apcatb.2014.06.040.
[11] S. Martin, P.L. Garcia-Ybarra, J.L. Castillo, Ten-fold reduction from the state-of-the-art platinum loading of electrodes prepared by electrospraying for high temperature proton exchange membrane fuel cells, Electrochem. Commun. 93 (2018) 57–61, https://doi.org/10.1016/j.elecom.2018.06.007.
[12] M.M. Whiston, I.L. Azevedo, S. Litster, K.S. Whitefoot, C. Samaras, J.F. Whitacre, Expert assessments of the cost and expected future performance of proton exchange membrane fuel cells for vehicles, Proc. Natl. Acad. Sci. 116 (2019) 4899–4904, https://doi.org/10.1073/pnas.1804221116.
[13] M. Carmo, G.P. Keeley, D. Holtz, T. Grube, M. Robinius, M. Müller, D. Stolten, PEM water electrolysis: innovative approaches towards catalyst separation, recovery and recycling, Int. J. Hydrog. Energy 44 (2019) 3450–3455, https://doi.org/10.1016/j.ijhydene.2018.12.030.
[14] L. Duclos, Environmental assessment of proton exchange membrane fuel cell platinum catalyst recycling, J. Clean. Prod. 142 (2017) 2618–2628, https://doi.org/10.1016/j.jclepro.2016.10.197.
[15] R. Sharma, S.J. Andreasen, J. Chamier, S.M. Andersen, Pt/C electrocatalyst synthesis from recycling of the spent PEMFC membrane electrode assembly: a closed loop circular economy, J. Electrochem. Soc. 166 (2019) F963–F970, https://doi.org/10.1149/2.0671913jes.
[16] A.S. Bandarenka, Exploring the interfaces between metal electrodes and aqueous electrolytes with electrochemical impedance spectroscopy, Analyst 138 (2013) 5540–5554, https://doi.org/10.1039/C3AN00791J.
[17] G. Doo, J.H. Lee, S. Yuk, S. Choi, D.-H. Lee, D.W. Lee, H.G. Kim, S.H. Kwon, S. G. Lee, H.-T. Kim, Tuning the ionomer distribution in the fuel cell catalyst layer with scaling the ionomer aggregate size in dispersion, ACS Appl. Mater. Interfaces 10 (2018) 17835–17841, https://doi.org/10.1021/acsami.8b01751.
[18] S.S. Kocha, K. Shinozaki, J.W. Zack, D.J. Myers, N.N. Kariuki, T. Nowicki, V. Stamenkovic, Y. Kang, D. Li, D. Papageorgopoulos, Best practices and testing protocols for benchmarking ORR activities of fuel cell electrocatalysts using rotating disk electrode, Electrocatalysis 8 (2017) 366–374, https://doi.org/10.1007/s12678-017-0378-6.
[19] R.W. Lindström, K. Kortsdottir, M. Wesselmark, A. Oyarce, C. Lagergren, Gr Lindbergh, Active area determination of porous Pt electrodes used in polymer electrolyte fuel cells: temperature and humidity effects, J. Electrochem. Soc. 157 (2010) B1795, https://doi.org/10.1149/1.3494220.
[20] M. Watt-Smith, J. Friedrich, S. Rigby, T. Ralph, F. Walsh, Determination of the electrochemically active surface area of Pt/C PEM fuel cell electrodes using different adsorbates, J. Phys. D Appl. Phys. 41 (2008), 174004, https://doi.org/10.1088/0022-3727/41/17/174004.
[21] T.R. Garrick, T.E. Moylan, M.K. Carpenter, A. Kongkanand, Editors' choice—electrochemically active surface area measurement of aged Pt alloy catalysts in PEM fuel cells by CO stripping, J. Electrochem. Soc. 164 (2016) F55–F59, https://doi.org/10.1149/2.0381702jes.

[22] M. Shao, J.H. Odell, S.-I. Choi, Y. Xia, Electrochemical surface area measurements of platinum- and palladium-based nanoparticles, Electrochem. Commun. 31 (2013) 46–48, https://doi.org/10.1016/j.elecom.2013.03.011.
[23] S. Trasatti, O. Petrii, Real surface area measurements in electrochemistry, J. Electroanal. Chem. 327 (1992) 353–376, https://doi.org/10.1016/0022-0728(92)80162-W.
[24] T. Binninger, E. Fabbri, R. Kötz, T.J. Schmidt, Determination of the electrochemically active surface area of metal-oxide supported platinum catalyst, J. Electrochem. Soc. 161 (2013) H121–H128, https://doi.org/10.1149/2.055403jes.
[25] M. Łukaszewski, M. Soszko, A. Czerwiński, Electrochemical methods of real surface area determination of noble metal electrodes–an overview, Int. J. Electrochem. Sci. 11 (2016) 4442–4469, https://doi.org/10.20964/2016.06.71.
[26] J.H. Jung, H.J. Park, J. Kim, S.H. Hur, Highly durable Pt/graphene oxide and Pt/C hybrid catalyst for polymer electrolyte membrane fuel cell, J. Power Sources 248 (2014) 1156–1162, https://doi.org/10.1016/j.jpowsour.2013.10.055.
[27] V.E. Guterman, A.Y. Pakharev, N.Y. Tabachkova, Microstructure and size effects in Pt/C and Pt3Ni/C electrocatalysts synthesized in solutions based on binary organic solvents, Appl. Catal., A 453 (2013) 113–120, https://doi.org/10.1016/j.apcata.2012.11.041.
[28] K.J.J. Mayrhofer, D. Strmcnik, B.B. Blizanac, V. Stamenkovic, M. Arenz, N. M. Markovic, Measurement of oxygen reduction activities via the rotating disc electrode method: from Pt model surfaces to carbon-supported high surface area catalysts, Electrochim. Acta 53 (2008) 3181–3188, https://doi.org/10.1016/j.electacta.2007.11.057.
[29] S.C. Ball, S.L. Hudson, D. Thompsett, B. Theobald, An investigation into factors affecting the stability of carbons and carbon supported platinum and platinum/cobalt alloy catalysts during 1.2V potentiostatic hold regimes at a range of temperatures, J. Power Sources 171 (2007) 18–25, https://doi.org/10.1016/j.jpowsour.2006.11.004.
[30] H.-S. Choo, T. Kinumoto, M. Nose, K. Miyazaki, T. Abe, Z. Ogumi, Electrochemical oxidation of highly oriented pyrolytic graphite during potential cycling in sulfuric acid solution, J. Power Sources 185 (2008) 740–746, https://doi.org/10.1016/j.jpowsour.2008.07.086.
[31] D. Schonvogel, J. Hülstede, P. Wagner, A. Dyck, C. Agert, M. Wark, Durability of electrocatalysts for ORR: Pt on nanocomposite of reduced graphene oxide with FTO versus Pt/C, J. Electrochem. Soc. 165 (2018) F3373–F3382, https://doi.org/10.1149/2.0361806jes.
[32] M. Sakthivel, J.-F. Drillet, An extensive study about influence of the carbon support morphology on Pt activity and stability for oxygen reduction reaction, Appl. Catal. B Environ. 231 (2018) 62–72, https://doi.org/10.1016/j.apcatb.2018.02.050.
[33] R. Sharma, Y. Wang, F. Li, J. Chamier, S.M. Andersen, Particle size-controlled growth of carbon-supported platinum nanoparticles (Pt/C) through water-assisted polyol synthesis, ACS Omega 4 (2019) 15711–15720, https://doi.org/10.1021/acsomega.9b02351.
[34] R. Sharma, Y. Wang, F. Li, J. Chamier, S.M. Andersen, Synthesis of a Pt/C electrocatalyst from a user-friendly Pt precursor (ammonium hexachloroplatinate) through microwave-assisted polyol synthesis, ACS Appl. Energy Mater. 2 (2019) 6875–6882, https://doi.org/10.1021/acsaem.9b01336.
[35] M. Tsuji, M. Hashimoto, Y. Nishizawa, M. Kubokawa, T. Tsuji, Microwave-assisted synthesis of metallic nanostructures in solution, Chem. Eur. J. 11 (2005) 440–452, https://doi.org/10.1002/chem.200400417.
[36] N.E. Sahin, T.W. Napporn, L. Dubau, F. Kadirgan, J.-M. Léger, K.B. Kokoh, Temperature-dependence of oxygen reduction activity on Pt/C and PtCr/C electrocatalysts synthesized from microwave-heated diethylene glycol method, Appl. Catal. B Environ. 203 (2017) 72–84, https://doi.org/10.1016/j.apcatb.2016.09.026.
[37] M. Chourashiya, R. Sharma, S.M. Andersen, Accurate determination of catalyst loading on glassy carbon disk and its impact on thin film rotating disk electrode for oxygen reduction reaction, Anal. Chem. 90 (2018) 14181–14187, https://doi.org/10.1021/acs.analchem.8b02697.
[38] H. Shang, Y. Lu, F. Zhao, C. Chao, B. Zhang, H. Zhang, Preparing high surface area porous carbon from biomass by carbonization in a molten salt medium, RSC Adv. 5 (2015) 75728–75734, https://doi.org/10.1039/C5RA12406A.
[39] T. Ungár, J. Gubicza, G. Ribárik, C. Pantea, T.W. Zerda, Microstructure of carbon blacks determined by X-ray diffraction profile analysis, Carbon 40 (2002) 929–937, https://doi.org/10.1016/S0008-6223(01)00224-X.
[40] R. Sharma, S. Gyergyek, J. Chamier, P. Morgen, S.M. Andersen, Pt/C electrocatalyst durability enhancement by inhibition of Pt nanoparticle growth through microwave pretreatment of carbon support, ChemElectroChem 8 (2021) 1183–1195, https://doi.org/10.1002/celc.202100226.
[41] C. Buttersack, Modeling of type IV and V sigmoidal adsorption isotherms, Phys. Chem. Chem. Phys. 21 (2019) 5614–5626, https://doi.org/10.1039/C8CP07751G.
[42] L. Castanheira, W.O. Silva, F.H.B. Lima, A. Crisci, L. Dubau, F. Maillard, Carbon corrosion in proton-exchange membrane fuel cells: effect of the carbon structure, the degradation protocol, and the gas atmosphere, ACS Catal. 5 (2015) 2184–2194, https://doi.org/10.1021/cs501973j.
[43] A.P. Hitchcock, V. Berejnov, V. Lee, M. West, V. Colbow, M. Dutta, S. Wessel, Carbon corrosion of proton exchange membrane fuel cell catalyst layers studied by scanning transmission X-ray microscopy, J. Power Sources 266 (2014) 66–78, https://doi.org/10.1016/j.jpowsour.2014.04.119.
[44] P. Kanninen, B. Eriksson, F. Davodi, M.E.M. Buan, O. Sorsa, T. Kallio, R. W. Lindström, Carbon corrosion properties and performance of multi-walled carbon nanotube support with and without nitrogen-functionalization in fuel cell electrodes, Electrochim. Acta 332 (2020), 135384, https://doi.org/10.1016/j.electacta.2019.135384.
[45] A. Riese, D. Banham, S. Ye, X. Sun, Accelerated stress testing by rotating disk electrode for carbon corrosion in fuel cell catalyst supports, J. Electrochem. Soc. 162 (2015) F783–F788, https://doi.org/10.1149/2.0911507jes.
[46] M.R. Tarasevich, V.A. Bogdanovskaya, N.M. Zagudaeva, Redox reactions of quinones on carbon materials, J. Electroanal. Chem. Interf. Electrochem. 223 (1987) 161–169, https://doi.org/10.1016/0022-0728(87)85257-9.
[47] W. Li, A.M. Lane, Resolving the HUPD and HOPD by DEMS to determine the ECSA of Pt electrodes in PEM fuel cells, Electrochem. Commun. 13 (2011) 913–916, https://doi.org/10.1016/j.elecom.2011.05.028.
[48] R. Sharma, S.M. Andersen, Quantification on degradation mechanisms of polymer electrolyte membrane fuel cell catalyst layers during an accelerated stress test, ACS Catal. 8 (2018) 3424–3434, https://doi.org/10.1021/acscatal.8b00002.
[49] Z.-Y. Zhou, X. Kang, Y. Song, S. Chen, Enhancement of the electrocatalytic activity of Pt nanoparticles in oxygen reduction by chlorophenyl functionalization, Chem. Commun. 48 (2012) 3391–3393, https://doi.org/10.1039/C2CC17945H.
[50] R. Sharma, S.M. Andersen, An opinion on catalyst degradation mechanisms during catalyst support focused accelerated stress test (AST) for proton exchange membrane fuel cells (PEMFCs), Appl. Catal. B Environ. 239 (2018) 636–643, https://doi.org/10.1016/j.apcatb.2018.08.045.
[51] S.T. Dix, S. Lu, S. Linic, Critical practices in rigorously assessing the inherent activity of nanoparticle electrocatalysts, ACS Catal. 10 (2020) 10735–10741, https://doi.org/10.1021/acscatal.0c03028.
[52] S. Moniri, T. Van Cleve, S. Linic, Pitfalls and best practices in measurements of the electrochemical surface area of platinum-based nanostructured electro-catalysts, J. Catal. 345 (2017) 1–10, https://doi.org/10.1016/j.jcat.2016.11.018.
[53] S. Rudi, C. Cui, L. Gan, P. Strasser, Comparative study of the electrocatalytically active surface areas (ECSAs) of Pt alloy nanoparticles evaluated by hupd and CO-stripping voltammetry, Electrocatalysis 5 (2014) 408–418, https://doi.org/10.1007/s12678-014-0205-2.